Aust. J. Phys., 1992, **45**, 263–91

Attachment of Electrons to Molecules at meV Resolution*

D. Klar, M.-W. Ruf and H. Hotop

Fachbereich Physik, Universität Kaiserslautern,
D-6750 Kaiserslautern, Federal Republic of Germany.

Abstract

A selective discussion of electron attachment to molecules is presented with emphasis on recent studies of SF_6, carried out with a novel laser photoelectron attachment (LPA) method in the energy range 0·1–170 meV with an effective energy resolution around 0·1 meV near threshold.

1. Introduction and Theoretical Background

Attachment of electrons to molecules XY is an important basic collision process, which is also of practical importance, e.g. in connection with the dielectric strength of gaseous media (Christophorou 1984). The collision cross sections for electron attachment are most significant at low electron energies $E \lesssim 15$ eV (Christophorou *et al.* 1982). The process is resonant in character and can be viewed to occur in two steps, involving the formation of an excited temporary negative ion XY^{-*}, which can decay into several possible final states in a way which depends on the molecule, on the electron energy, and on the particle densities in the investigated system:

$$e^-(E) + XY \rightarrow XY^{-*} \longrightarrow XY(v) + e^-(E') \quad (1a)$$

$$\xrightarrow{\text{DA}} X^- + Y \quad (1b)$$

$$\xrightarrow{\tau \gtrsim 10^{-5}\ \text{s}} XY^{-*} \quad (1c)$$

$$\xrightarrow{\text{RA}} XY^- + \gamma \quad (1d)$$

$$\xrightarrow[(+M)]{\text{TBA}} XY^- . \quad (1e)$$

Path (1a) corresponds to elastic or inelastic electron scattering, mediated by the negative ion resonance XY^{-*}, which is formed in the primary attachment process. In process (1b) dissociative attachment (DA) occurs, while in path (1c) a metastable negative ion XY^{-*} persists for times long enough to allow its detection

* Paper presented at the Joint Symposium on Electron and Ion Swarms and Low Energy Electron Scattering, held at Bond University, Queensland, 18–20 July 1991.

0004-9506/92/030263$05.00

with a mass spectrometer ($\tau \gtrsim 10\ \mu s$). A very important example for reaction (1c) involves $XY = SF_6$, which will also be the main topic of this paper. For sufficiently long-lived resonance states, stabilisation by photon emission (radiative attachment, RA) may occur, as indicated in (1d). At sufficiently high densities of either XY or another gas M, which can act as a third body for collisional stabilisation within the lifetime of XY^{-*}, three body attachment (TBA) will play an important role.

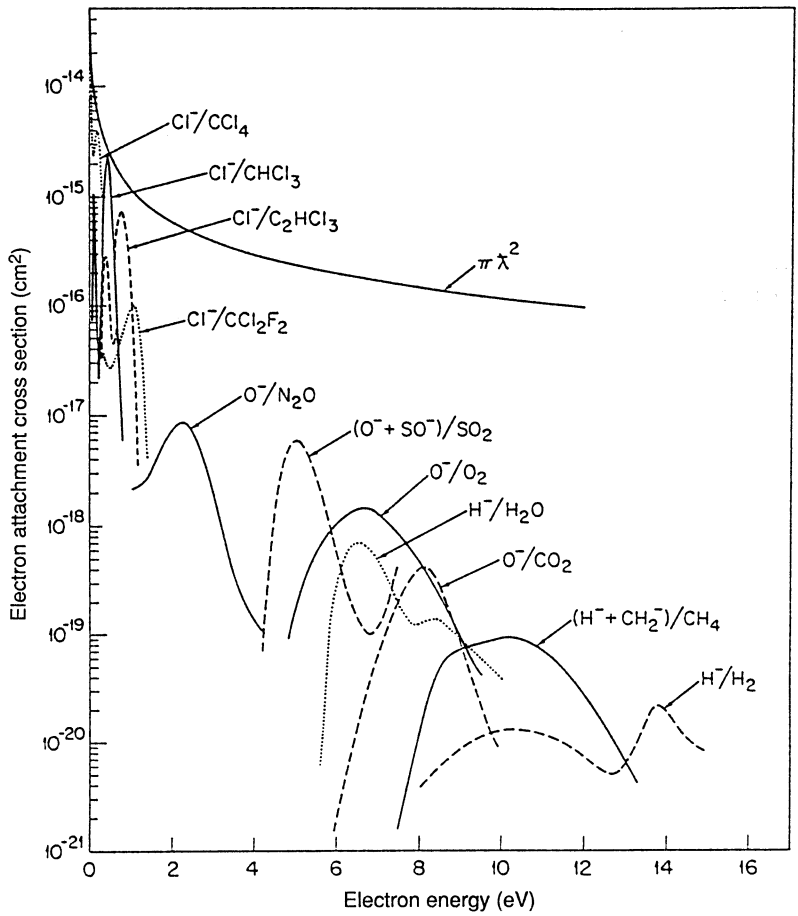

Fig. 1. Absolute cross sections for dissociative attachment of electrons by small molecules in the energy range 0–16 eV [from Christophorou *et al.* (1982) with permission].

In most cases, dissociative attachment is the dominant process for the capture of electrons, and Fig. 1 summarises DA cross sections measured for some simple molecules in their electronic ground state in the energy range 0–15 eV (Christophorou *et al.* 1982). At energies above 2 eV, typical DA cross sections are in the range 10^{-17}–10^{-19} cm^2 and correspond to capture into repulsive negative ion states according to the respective Franck–Condon overlaps. At low energies ($\lesssim$1 eV), much higher DA cross sections are found for many (especially halogen-containing) molecules; they can get close to the de Broglie cross section

$\sigma_0 = \pi\lambda^2$ for s-wave ($L = 0$) capture, which is drawn as the uppermost curve in Fig. 1.

In the limit of zero kinetic energy, the physics of threshold laws for capture in long-range potentials $V(r)$, which decrease more rapidly than $1/r^2$ at large distances between the electron and the target molecule, requires the following basic energy dependence of the cross section $\sigma_e(E)$ for attachment of an electron in a partial wave with orbital angular momentum L (Bethe 1935; Wigner 1948):

$$\sigma_e(E;\, L) \underset{E \to 0}{\sim} E^{L-1/2} . \tag{2}$$

The dependence on L reflects the fact that for the potentials considered the centrifugal part of the effective potential is dominant at large distances and therefore is mainly responsible for the penetration of the wavefunction into the region of capture. For s-waves ($L = 0$), the attachment cross section is inversely proportional to the electron velocity v,

$$\sigma_e(E;\, L{=}0) \underset{E \to 0}{\sim} E^{-1/2} \sim v^{-1} , \tag{3}$$

and exhibits the same behaviour as the one for neutron capture by nuclei (Bethe 1935). This $1/v$ law can be understood by considering the attachment probabilities p_{att}: on the one hand $p_{att} \sim |\Psi_0|^2$ for low energies and de Broglie wavelengths λ large compared with the target diameter, on the other hand one has (from the definition of the cross section and the electron flux density $j_e = n_e v$) $p_{att} \sim \sigma_e j_e = \sigma_e v |\Psi_0|^2$, i.e. $\sigma_e v \approx$ const. as required by (3).

For electron velocities confined to the validity range of (3), the rate constant $k_e \equiv \langle \sigma_e(v) v \rangle$ for electron attachment involving s-wave capture is predicted to be a constant k_0:

$$k_e = \int \sigma_e(v)\, v f(v)\, \mathrm{d}v = k_0 , \tag{4}$$

where $f(v)$ is the normalised velocity distribution function of the slow electrons. Vogt and Wannier (1954) presented a general discussion on capture of charged particles interacting with a target through the polarisation potential; for electrons we have

$$V_{pol}(r) = -\frac{\alpha e^2}{8\pi\epsilon_0 r^4} , \tag{5}$$

where α is the dipole polarisability of the target and e is the electron charge. In the classical region (i.e. where many angular momenta L contribute to capture), Vogt and Wannier (1954) quantum mechanically recovered the well-known classical Langevin formula (1905) for the capture cross section $\sigma_c \sim (\alpha/E)^{1/2}$, which leads to an energy-independent rate constant. In their analysis of the cross section at very low energies, Vogt and Wannier showed that the basic behaviour $\sigma_c \sim (\alpha/E)^{1/2}$ persists even in the limit $E \to 0$, but that the absolute value of the limiting s-wave capture cross section $\sigma_c(E{\to}0)$ is twice as large as the Langevin cross section:

$$\sigma_c(E \to 0) = 4\pi a_0^2 (\alpha/2E)^{1/2} , \tag{6}$$

with α, E in atomic units and the Bohr radius $a_0 = 0{\cdot}529177{\times}10^{-10}$ m.

From (6) we obtain the prediction for the limiting s-wave electron capture rate constant (α in atomic units of a_0^3):

$$k_c(E \to 0) = 7{\cdot}755 \times 10^{-8}\, \alpha^{1/2}\ \mathrm{cm^3\,s^{-1}}. \tag{7}$$

Moreover, an estimate for the range of validity of (6) and (7) can be inferred from Fig. 3 in the paper of Vogt and Wannier (1954), namely $(8\alpha E)^{1/4} < 0{\cdot}5$. Because of the absence of electric dipole and quadrupole moments, the molecule $XY = SF_6$ is well-suited for a test of the predictions (6) and (7) by studying reaction (1c) at very low energies. From the well-known polarisability $\alpha(SF_6) = 44{\cdot}1a_0^3$ (Nelson and Cole 1971) we calculate $k_c(E{\to}0) = 5{\cdot}15{\times}10^{-7}\ \mathrm{cm^3\,s^{-1}}$, expected to be valid for energies below about 3 meV.

So far, the most advanced experiments on threshold attachment of free electrons have been carried out by Chutjian and colleagues (Chutjian *et al.* 1984, 1985, 1987; Chutjian 1992), who used VUV photoionisation of Kr atoms above the $^2P_{1/2}$ threshold to generate photoelectrons of defined and variable energy. With an effective electron energy width of 4–8 meV (FWHM), they studied relative attachment cross sections for a variety of molecules in the range 0–150 meV and produced absolute cross sections by normalisation to rate constants obtained in swarm experiments (Chutjian and Alajajian 1985). For several molecules Chutjian *et al.* (1984, 1985, 1987) interpreted a strong peak in their measured negative ion yields close to zero energy as evidence for, and to be compatible with, the $E^{-1/2}$ rise expected for s-wave attachment at energies $\lesssim 10$ meV.

As an interesting alternative to the use of free electrons, several groups and most notably Dunning and colleagues (Dunning 1987 and references therein) studied attachment reactions involving electron transfer from Rydberg atoms A^{**} (nl):

$$A^{**}(n\ell) + XY \longrightarrow A^+ + XY^-(X^- + Y). \tag{8}$$

For sufficiently high values of the principal quantum number n, the Rydberg electron may be viewed to act as a (quasi) free electron with an average kinetic energy $\langle E\rangle_{n\ell}$ equal to the (negative) binding energy ($\langle E\rangle_{n\ell} = |E_{n\ell}| = 13{\cdot}6/n^{*2}$ eV, n^* = effective principal quantum number), and the presence of the ion core A^+ may be neglected. Note that at high n and for thermal collision energies of the A^{**} $-XY$ system ($E_{rel} \approx 50$ meV), all the ion pairs $A^+{-}XY^-$, which are created at electron transfer distances of about $R_t \approx \langle r\rangle_{n\ell} = \frac{3}{2}n^{*2}a_0$, can escape from the attractive Coulomb potential, since the kinetic energy E_{rel} is significantly larger than the absolute value of the Coulomb energy at R_t. Therefore, the cross section and the rate constant for the ion-pair formation reaction (8) should be equal to the respective quantities for the primary electron transfer. In the framework of the quasi-free electron model for reactions of Rydberg electrons (see e.g. Matsuzawa 1983) the rate constant $k_{n\ell}$ for electron transfer from A^{**} $(n\ell)$ to XY can be written as

$$k_{n\ell} = \int k_e(v)\, g_{n\ell}(v)\, \mathrm{d}v\,. \tag{9}$$

Here $g_{n\ell}(v)$ represents the normalised velocity distribution of the Rydberg electron. For sufficiently high n and in cases in which s-wave attachment occurs (i.e. $L = 0$ of the Rydberg electron with respect to the target molecule XY), the dominant contributions to the integral stem from velocities v for which $k_e(v) = \text{const.} = k_0$, and therefore one expects $k_{n\ell} \approx k_0$, i.e. the rate constants for negative ion formation in s-wave attachment reactions involving free electrons and high n Rydberg electrons should be the same. Dunning and colleagues (Zollars *et al.* 1985; Dunning 1987) have provided substantial evidence for this equivalence to hold at $n \gtrsim 35$ in cases such as $XY = SF_6$, CCl_4.

In the present paper, we discuss recent high resolution threshold attachment studies and concentrate on the important case $XY = SF_6$. We briefly present the experimental methods and discuss pertinent experimental results, obtained by the VUV and our newly developed laser photoelectron method as well as in Rydberg atom collisions. It will be seen that—in agreement with the expectation based on the work of Vogt and Wannier (1954)—the limiting $E^{-1/2}$ dependence for s-wave attachment is only reached at very low energies ($\lesssim$1 meV). The rate constants for free and Rydberg electron attachment will be found to agree well at the present level of accuracy (25%). Our free electron data, measured over the range 0–200 meV with sub-meV resolution, in addition reveal prominent threshold structure at the onset for ν_1 vibrational excitation of SF_6, similar to the behaviour of the attachment cross section theoretically predicted by Gauyacq and Herzenberg (1984).

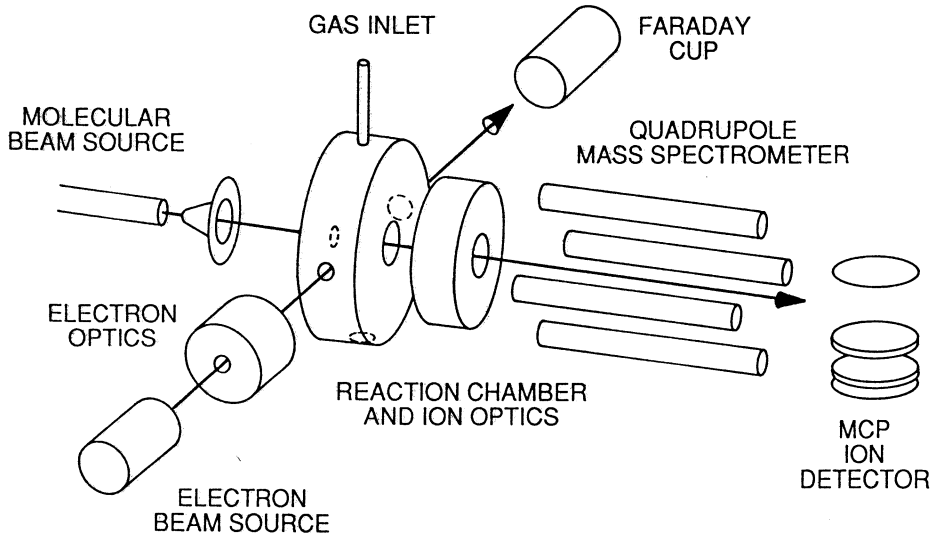

Fig. 2. Semi-schematic representation of apparatus for electron attachment experiments.

2. Experimental Aspects

A typical experimental setup for electron attachment studies at low densities is shown in Fig. 2. It consists of an energy-selected and energy-variable electron source, a reaction chamber with the molecular target, a mass-resolving negative ion detector, and a data acquisition system for recording energy-dependent attachment cross sections. Most of the previous work was carried out with a conventional

electron gun providing low to medium energy resolution ($\Delta E \gtrsim 50$ meV) (Schultz 1973; Kline *et al.* 1979; Oster *et al.* 1989; Märk 1991).

More recently, quasi-monoenergetic electron sources, based on controlled photoelectron production, were developed for use in electron scattering (Kennerly *et al.* 1981; Field *et al.* 1988, 1991) and in electron attachment (Ajello and Chutjian 1979; Chutjian *et al.* 1984, 1985). In a basic paper, Gallagher and York (1974) addressed the relevant aspects of such sources and described a cw laser photoionisation scheme involving metastable Ba* atoms to generate monoenergetic electrons of fixed low energy (17 meV) at high brightness. More recently, Field *et al.* (1988, 1991) used monochromatised synchrotron radiation to photoionise Ar at the ($11s'$, J=1) autoionisation resonance and thereby produced very slow electrons ($\approx$4 meV), which were efficiently drawn out with a weak electric field, accelerated and used for elastic and inelastic electron scattering studies from a nozzle target beam at a typical resolution around 4 meV.

In their TPSA method (threshold photoelectron spectroscopy by electron attachment), Chutjian and colleagues used monochromatised VUV radiation to photoionise ground state Xe or Kr atoms at and above the respective $^2P_{1/2}$ (i.e. the higher lying) fine structure thresholds, thereby generating photoelectrons of variable energy and with an energy resolution determined mainly by the monochromator slit width. Their choice of the $^2P_{1/2}$ threshold was motivated by the short lifetime of the autoionising Rydberg levels in the series (ns', J=1) and (nd', J=1), which converge to the $^2P_{1/2}$ limit. Even at $n \approx 100$, the lifetimes of the relatively sharp and long-lived (ns', J=1) levels are as short as 5 ns (Klar *et al.* 1991) and therefore autoionise with the emission of fast electrons, which are inefficient for threshold attachment. In the region below zero energy, the data of Chutjian *et al.* (1984, 1985, 1987) are therefore free of signals which would occur below the $^2P_{3/2}$ threshold as a result of electron transfer reactions involving long-lived Rydberg atoms. Chutjian *et al.* employed a weak electric field to draw out the negative product ions from the reaction zone with a special field penetration lens system. In their recent studies they achieved a typical overall energy resolution (FWHM) of 6–8 meV (Chutjian *et al.* 1984, 1985, 1987, 1992). Due to the low monochromatised VUV photon flux, rather high densities of the rare gas and the attachment target had to be used to achieve sufficient electron current and negative ion signal; for example, in their work on $XY = SF_6$, to be discussed below, they employed $4{\cdot}5\times10^{-3}$ mbar of Kr and $1{\cdot}3\times10^{-4}$ mbar of XY (Chutjian and Alajajian 1985).

Based on our experience with resonant two-photon excitation and ionisation of metastable rare gas atoms (Ganz *et al.* 1982, Harth *et al.* 1987; Schohl *et al.* 1991), we have developed a novel laser photoelectron method (see Fig. 3) for electron attachment studies at sub-meV resolution (Klar *et al.* 1992). As in the work of Chutjian *et al.* (1984, 1985), the basic idea is the controlled production of energy-variable photoelectrons with a wavelength-tunable light source. In contrast to the previous work we use lasers to photoionise a low density target of metastable $Ar^*(4s\,^3P_2)$ atoms ($\approx3\times10^6$ cm^{-3}; see Schohl *et al.* 1991) in a well-collimated beam from a differentially-pumped dc discharge source in a field-free region (magnetic fields are $\lesssim6\times10^{-7}$ T), applying pulsed electric fields for ion detection. As indicated in Fig. 3 (left) we have chosen a resonant two-photon excitation–ionisation scheme, involving the closed transition

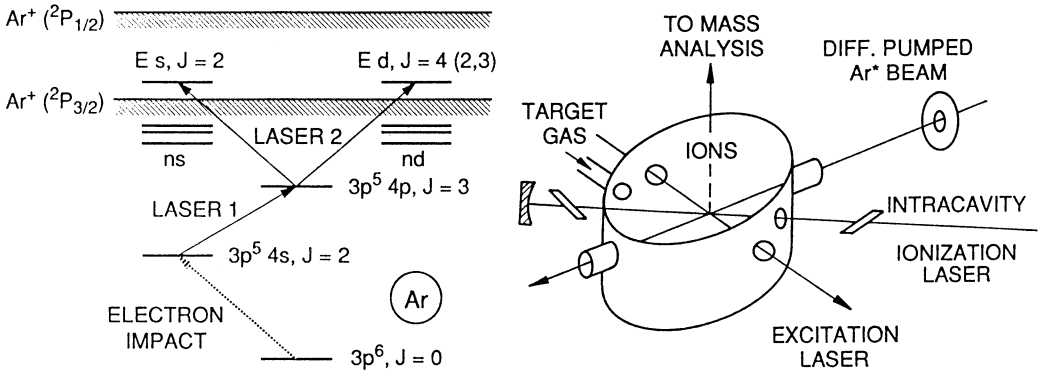

Fig. 3. Illustration of the principle (left) and the experimental realisation (right) of the laser photoelectron attachment (LPA) method.

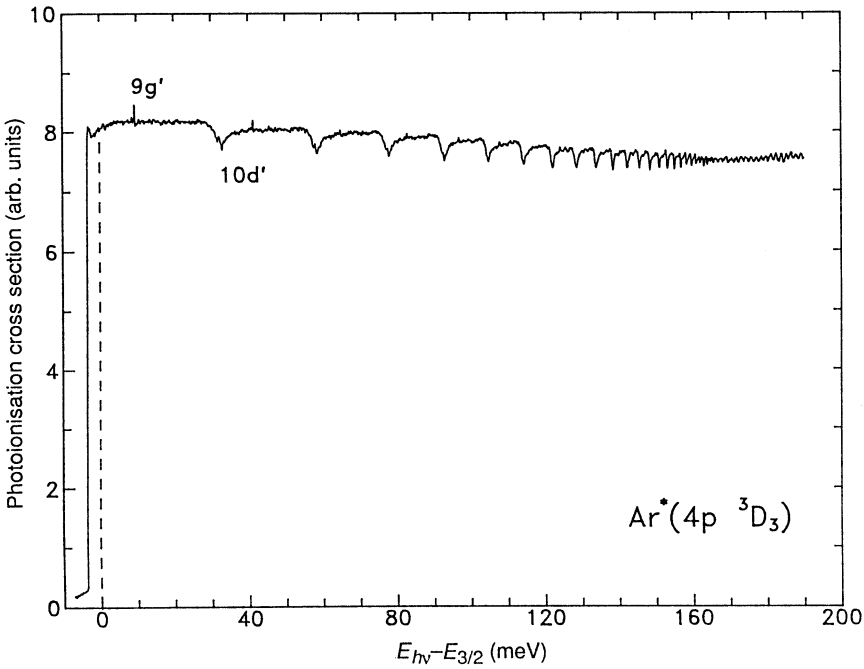

Fig. 4. Energy dependence of the total cross section for photoionisation of polarised Ar* ($4p\,^3D_3$) atoms. The energy scale represents the photoelectron energy above the $Ar^+(^2P_{3/2})$ threshold $E_{3/2}$. The signal below threshold is induced by field ionisation of Rydberg states in the static electric field ($23\ V\,cm^{-1}$), used to extract the photoions into the mass spectrometer in this experiment. The polarisation directions of the two linearly-polarised lasers, used to excite the transition $Ar^*(4s\,^3P_2–4p\,^3D_3)$ and to ionise the $Ar^*(4p\,^3D_3)$ atoms, were chosen parallel; under these conditions, the (nd') and (ng') autoionisation resonances are especially weak features.

$4s\,^3P_2$–$4p\,^3D_3$ as the first step. This approach has four advantages: (i) It is state selective [$Ar^*(4s\,^3P_0)$ atoms also present in the atomic beam are not excited]. (ii) It is more efficient than one photon ionisation of $Ar^*(4s\,^3P_2)$ atoms since the photoionisation cross section for $Ar^*(4p\,^3D_3)$ atoms ($\approx 8\times10^{-18}$ cm^2; see Chang and Kim 1982) is at least a factor of 10 higher than that for $Ar^*(4s\,^3P_2)$ atoms near threshold (Dunning and Stebbings 1974; Duzy and Hyman 1980). Note that nearly 50% of the $Ar^*(4s\,^3P_2)$ atoms are excited to the $Ar^*(4p\,^3D_3)$ level by Doppler-free, transverse pumping of this closed transition with a stabilised single-mode dye laser (811·75 nm). (iii) The threshold wavelength for $Ar^*(4p\,^3D_3)$ photoionisation (461·96 nm) is much more convenient than the one for $Ar^*(4s\,^3P_2)$ ionisation (294·41 nm); an efficient dye laser (Stilbene 3) can therefore be used in intracavity operation [typical intracavity power around 2 W, yielding $Ar^*(4p\,^3D_3)$ photoionisation efficiencies around 0·6%; see Schohl *et al.* (1991)]. (iv) The photoionisation cross section for $Ar^*(4p\,^3D_3)$ is nearly constant and autoionisation resonances (nd', ng') are only weakly excited because of the $^2P_{3/2}$ character of the ion core in the $Ar^*(4p\,^3D_3)$ level. Especially for parallel linear polarisations of the two lasers (used in all our attachment experiments), the contribution due to resonances is very low, as can be judged from Fig. 4; the continuum oscillator strength of these resonances amounts to only about 1% as compared with that for direct 4p ionisation into the $Ar^+(^2P_{3/2})$ continuum.

Under typical experimental conditions [$Ar^*(4s\,^3P_2)$ flux about 10^9 s^{-1}] the photoelectron current is about 10^{-12} A; it originates from a volume of about 1 mm^3, which on average contains about 10 photoions. In most experiments, the frequency width of the ionising laser, as limited by a three-plate birefringent filter, was about 36 GHz (1·2 cm^{-1} = 0·15 meV); insertion of a thin (0·11 mm) fused-silica etalon reduced the bandwidth to 10 GHz (0·33 cm^{-1} = 40 μeV). It was expected that the overall resolution in the attachment experiments would be limited by stray electric fields (including space charge effects). An estimate of ion space charge can be obtained by calculating the potential variation $\Delta\Phi$ within a sphere of radius R, homogeneously charged with Q elementary charges: $\Delta\Phi\ (\mu\text{V}) \approx 0{\cdot}7Q/R\ (\text{mm})$. With $R = 0{\cdot}5$ mm and $Q \approx 10e$, one gets $\Delta\Phi \approx 14\ \mu$V; we therefore conclude that potential variations due to photoion space charge contribute less to the overall energy resolution than the bandwidth of the ionising laser.

In order to minimise the influence of stray electric fields we took three measures: (i) the reaction chamber, fabricated of demagnetised polished stainless steel, is of basically cylindrical symmetry (inner diameter 48 mm) with extension tubes in the direction of the atomic and laser beams and properly chosen collimating apertures to prevent field penetration into the reaction centre (see Fig. 5); (ii) all the surfaces surrounding the reaction region were covered with a layer of graphite to reduce potential variations on the walls; (iii) the potential supplies to the electrodes forming the reaction chamber and the electrical connections were properly chosen to minimise ripple and contact potential differences. Apart from these measures, the experiment most importantly is required to combine two demands, namely a field-free region during electron production and attachment followed by a sufficiently strong, pulsed electric field to accelerate the product ions towards the mass spectrometer. Therefore, the whole experiment is pulsed at a repetition rate of about 140 kHz; the timing sequence is indicated in Fig. 6. The

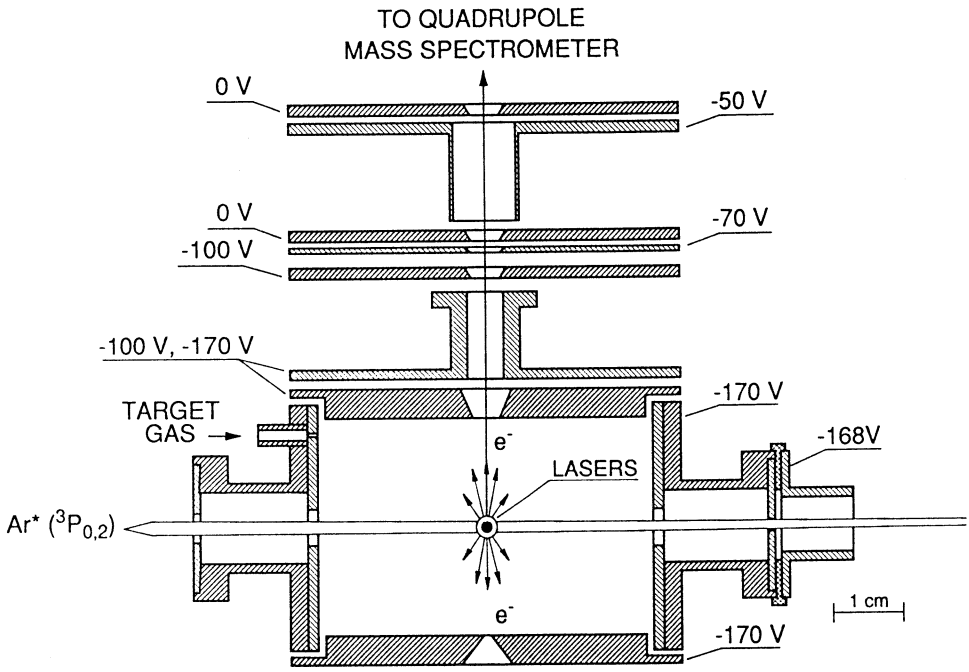

Fig. 5. Vertical cut through the reaction chamber and ion acceleration optics used in the LPA experiment. The potentials applied to the different electrodes are indicated; the potential on the upper plate and the following tube element is switched between −170 and −100 V for negative ion extraction (see timing diagram in Fig. 6).

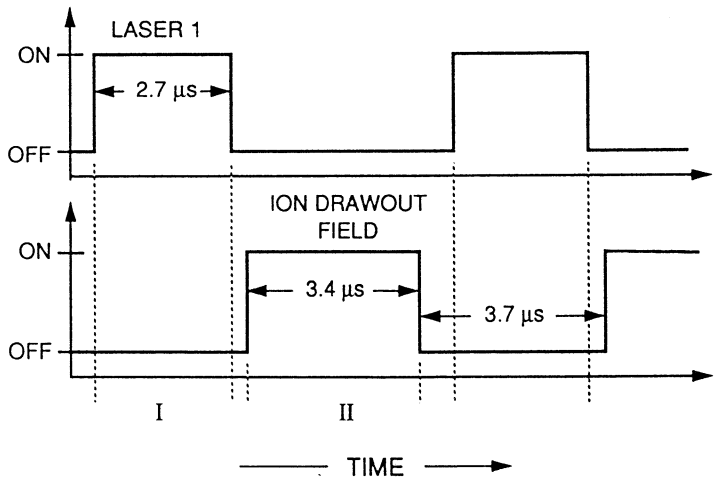

Fig. 6. Timing sequence for (I) pulsed electron production and attachment and (II) subsequent pulsed negative ion extraction, as used in the laser photoelectron attachment experiment.

excitation laser 1 is switched on and off by passage through an acousto-optical modulator, and the electron production follows this pulse sequence. Careful alignment of the ionising intracavity laser (for its design see Weissmann *et al.* 1984) eliminated the creation of spurious electrons at collimating apertures. A special RC filter in the lead to the extraction plates serves to obtain a smooth waveform for the extraction pulse (voltage 70 V and electric field 23 $\mathrm{V\,cm^{-1}}$). From an analysis of the apparent attachment yield at threshold, measured with a photon resolution of 40 μeV (FWHM) and to be discussed in Section 3, we can conclude that the setup described allows attachment experiments to be carried out at an effective electron energy resolution of 100 μeV or even below. The average stray electric fields consequently must have been 100 $\mu\mathrm{V\,mm^{-1}}$ or below (depending on the effective size of the attachment region). In such a low electric field F, the energy shift ΔE_F of the ionisation threshold towards lower energies, as estimated with the classical formula (see e.g. Harmin 1984)

$$\Delta E_F = 75\ \mu\mathrm{eV}[F\ (\mathrm{mV\,mm^{-1}})]^{1/2}, \tag{10}$$

would amount to only 24 μeV. We note, however, that our threshold data indicate that relation (10) overestimates the value of the electric field at a given measured energy shift ΔE_F, at least for low fields ($<1\ \mathrm{mV\,mm^{-1}}$); see Section 3*c*.

Apart from the influence of the laser bandwidth and stray electric fields on the electron energy width, there are kinematical effects which limit the resolution, namely the Doppler effect associated with the velocity of the electron source [$\bar{v}(\mathrm{Ar}) = 560\ \mathrm{m\,s^{-1}}$] on the one hand, and with the motion of the target gas on the other. In our study of SF_6, present as a diffuse gas at $T = 300$ K with an average velocity $\bar{v}(SF_6) \approx 200\ \mathrm{m\,s^{-1}}$, the Doppler effect due to the source motion dominates. The corresponding Doppler energy width ΔE_D (in meV), estimated with an isotropic photoelectron angular distribution, is given by $\Delta E_\mathrm{D}(E) \approx 0{\cdot}06E^{1/2}$, where E is the photoelectron energy in meV. At energies above about 10 meV the Doppler broadening provides the largest contribution to the effective electron energy width.

As a final point in this section, we discuss the procedure by which we determine energy-dependent attachment cross sections $\sigma_\mathrm{e}(E)$, and mention sources of systematic errors. In principle, the attachment yield $Y_\mathrm{e}(E) \sim \sigma_\mathrm{e}(E)$ can be determined in a direct way by taking the ratio of the attachment product current $I_\mathrm{e}(E)$ to the photoelectron or Ar^+–ion current $I_\gamma(E)$: $Y_\mathrm{e}(E) \sim I_\mathrm{e}(E)/I_\gamma(E)$. Variations of the experimental conditions (Ar^* beam, laser intensities, beam overlap) and energy dependent changes of the ionisation probability should not affect the current *ratio* (to first order). In our setup, simultaneous linear detection of both currents I_e and I_γ (extracted in opposite directions from the reaction region) and thereby the direct determination of the current ratio I_e/I_γ was not possible. In order to discriminate against spurious signals [e.g. Penning ions due to ionisation of background gas (O_2, H_2O) by laser-excited $Ar^*(4p\,^3D_3)$] and to identify the attachment product ions we used a quadrupole mass spectrometer for ion analysis, followed by an ion deflector and a dual channel plate ion detector in a chevron mount. The density of the molecular target was chosen sufficiently low to avoid saturation of the detector (ion counting rates $<5{\times}10^3\ \mathrm{s^{-1}}$) and adjusted to guarantee low attachment probability at all electron energies. With intracavity operation of the ionisation laser, the photoion current was too high

for unsaturated detection. Therefore, we chose the following scheme for the determination of the energy dependence of the attachment cross section:

(I) Accurate measurement of the energy dependence of the photoionisation cross section $\sigma_\gamma(E) \sim I_\gamma(E)/F_\gamma(\lambda)$ (see Fig. 4) using a single pass collimated laser beam (power $\approx$100 mW), extracted from a shortened (yet long) cavity. The photon flux F_γ was determined from the power $P_\gamma = F_\gamma E_\gamma$ ($E_\gamma = hc/\lambda$ = photon energy of ionisation laser), measured with a calibrated thermopile (Coherent Labmaster). Care was taken to avoid variations of the beam overlap as a function of wavelength. We estimate that the uncertainties of the (relative) photoionisation cross section do not exceed $\pm 2\%$ over the range shown in Fig. 4.

(II) Determination of the attachment yield $Y_e(E) \sim \sigma_e(E) \sim I_e(E)/F_\gamma^{IC}\,\sigma_\gamma(E)$ by means of the measured negative ion signal $I_e(E)$ and intracavity laser flux $F_\gamma^{IC}(\lambda)$ in combination with the photoionisation cross section $\sigma_\gamma(E)$. The ionising intracavity photon flux is related to the wavelength-dependent laser power $P_\gamma(\lambda)$, measured behind the terminating cavity mirror with the same thermopile used in experiment (I), by $F_\gamma^{IC}(\lambda) = 2P_\gamma(\lambda)/E_\gamma\, T(\lambda)$. Here $T(\lambda)$ is the wavelength-dependent transmission of the terminating mirror, measured with a spectrophotometer (Zeiss DMR 21) over the range of major interest (465–430 nm) with values $3{\cdot}1\% < T(\lambda) < 4{\cdot}7\%$ and uncertainties $\lesssim 4\%$. Note that a possible (yet weak) wavelength-dependent response of the thermopile detector [not included in the uncertainty for $\sigma_\gamma(E)$] does not influence the yield $Y_e(E)$, since the thermopile response function cancels out in the product $F_\gamma^{IC}(\lambda)\,\sigma_\gamma(E)$.

(III) Absolute attachment cross sections are derived from the measured yield $Y_e(E)$ (i.e. relative cross section) by normalisation to the well-known rate constant determined at $T = 300$ K in swarm experiments (see Section 3).

Apart from the uncertainty in the transmission function of the terminating mirror we mention two other sources of systematic errors, which together can be considered as the main factors which may limit the accuracy in our measured relative attachment cross sections: (i) variations of the overlap of the laser-excited $Ar^*(4p\,^3D_3)$ beam fraction with the intracavity ionisation laser as a function of its wavelength; (ii) effects due to energy-dependent angular distributions of the photoelectrons.

With regard to (i), the intrinsic pointing stability of the wavelength-tuned intracavity laser was observed to be very high (as occasionally monitored by distant observation of the laser beam, transmitted through the terminating mirror). Before data were taken, the overlap between the laser excited $Ar^*(4p\,^3D_3)$ atoms and the ionisation laser was carefully optimised. With these observations and measures the factor (i) introduces only small uncertainties, which cannot, however, be quantified.

With regard to point (ii), one may expect significant variations of the angular distribution of the photoelectrons, especially in the region of the autoionisation resonances, which, however, are rather weak features for the chosen parallel laser polarisations (see Fig. 4). Inspection of the attachment cross sections did not reveal any anomalies in the region of the $Ar^*(n\ell')$ resonances. As for variations of the angular distribution of the photoelectrons in the energy range 0–175 meV outside resonances, we have some information from measurements at selected wavelengths

in the range 458–413 nm (Schohl *et al.* 1992). The angular distributions obtained at $E = 23$, 144 and 318 meV with parallel linear polarisations of the lasers showed perpendicular anisotropies [expressed by the intensity ratio $I(\theta{=}90°)/I(\theta{=}0)$; θ is the angle between photoelectron momentum and laser polarisation directions] from 0·65 to 0·45. We conclude that energy-dependent variations of the photoelectron angular distribution are rather small; no experimental evidence exists that they introduce significant systematic errors in the measured attachment cross sections $\sigma_e(E)$.

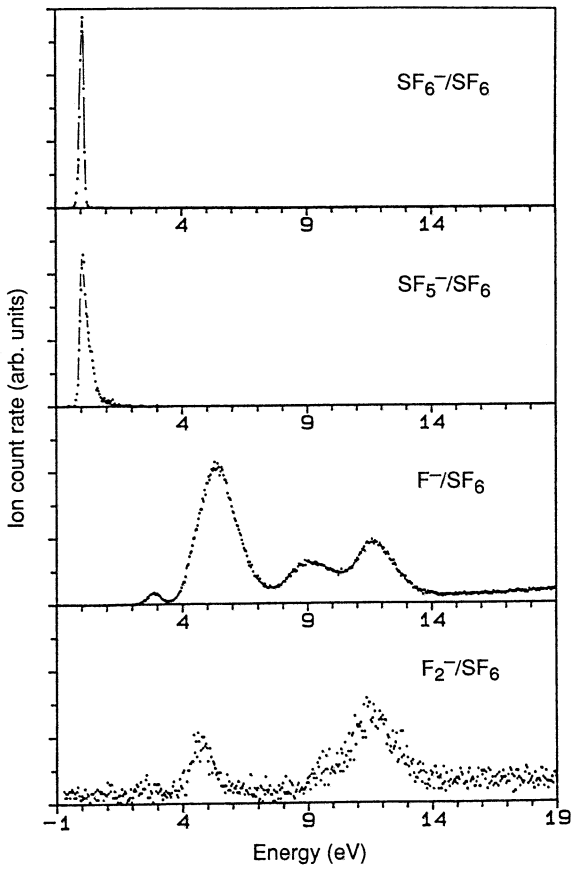

Fig. 7. Ion yield curves for four of the negative ion species formed by electron attachment to SF_6 in the energy range 0–19 eV [taken from Fenzlaff *et al.* (1988) with permission].

3. Results and Discussion

In this section we confine most of the discussion to the case $XY = SF_6$. We first survey some free electron results obtained with medium to high resolution, next dwell on Rydberg electron transfer data [including very recent results with principal quantum numbers as high as $n = 400$ (Ling *et al.* 1992)], and then discuss in detail our recent free electron attachment experiments, carried out with sub-meV resolution.

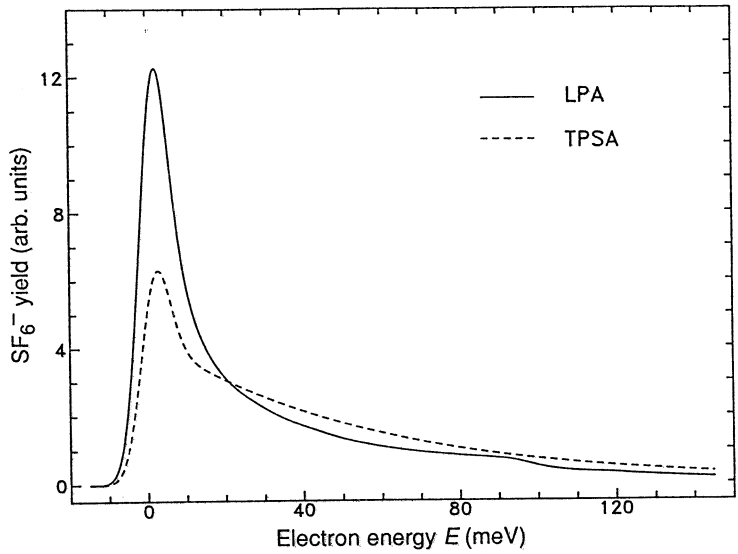

Fig. 8. SF_6^- yield for attachment of free electrons to SF_6 at energies below 140 meV. The dashed curve represents the TPSA results and the smooth curve corresponds to the LPA cross section, both convoluted with a Gaussian resolution function of 8 meV FWHM. The two results will be discussed in connection with Fig. 12.

(3a) Brief Survey of Previous Free Electron Attachment Experiments

Fig. 7 summarises energy-dependent attachment yields, reported by Fenzlaff *et al.* (1988) for the ions SF_6^-, SF_5^-, F^- and F_2^-. The SF_6^- ion yield shows a single sharp resolution-limited peak at zero energy, while the cross section for SF_5^- production peaks at about 0·35 eV with a value of $(4\text{–}5)\times10^{-16}$ cm^2 (Kline *et al.* 1979; Hunter *et al.* 1989). The yields for F^- and F_2^- exhibit several peaks with cross sections in the range $(1\text{–}50)\times10^{-19}$ cm^2 (Kline *et al.* 1979), pointing to the contribution from several different repulsive negative ion surfaces.

Employing their TPSA method, Chutjian and Alajajian (1985) measured the SF_6^- ion yield at $T = 300$ K with 8 meV resolution. The dashed curve in Fig. 8 represents their fitted attachment yield, involving an analytic cross section of the assumed form

$$\sigma_e(E) = N[a(E^{-1/2}e^{-E^2/\lambda^2}) + e^{-E/\gamma}], \tag{11}$$

with fitted parameters $a = 1{\cdot}951$ (meV)$^{1/2}$, $\lambda = 4{\cdot}5$ meV and $\gamma = 55{\cdot}9$ meV and convoluted with a spectrometer function of 8 meV width (FWHM). The cross section (11) represents a superposition of an s-wave threshold component, suppressed at energies above 5 meV, and an exponential decrease for higher energies. The factor N serves to establish an absolute cross section scale by normalisation to the thermal attachment rate constant at $T = 300$ K:

$$k_e(T) = (2/m)^{1/2} \int_0^\infty \sigma_e(E) E^{1/2} f(E;\, T)\, \mathrm{d}E\,, \tag{12}$$

with

$$f(E;\, T) = (2/\sqrt{\pi})\bar{E}^{-3/2}E^{1/2}\exp(-E/\bar{E}) \tag{13}$$

and $\bar{E} = k_B T = 25 \cdot 85$ meV ($T = 300$ K). Using $k_e(T{=}300\text{ K}) = 2 \cdot 27 \times 10^{-7}$ cm^3 s^{-1} (Petrović and Crompton 1985), Chutjian and Alajajian (1985) obtained $N = 4 \cdot 36 \times 10^{-14}$ cm^2. The resulting absolute TPSA attachment cross section will be shown in Fig. 12 (Section 3*c*).

The smooth curve in Fig. 8 represents the SF_6^- yield, obtained by convolution of our laser photoelectron attachment (LPA) cross section (Fig. 12) with a Gaussian resolution function of 8 meV FWHM. We postpone the comparison between the TPSA and LPA yields to the discussion connected with Fig. 12.

(3b) Electron Attachment in Rydberg Atom Collisions

As mentioned in the Introduction, the rate constant $k_{n\ell}$ for ion-pair formation in reaction (8) at high n should agree with the rate constant k_e for s-wave electron attachment within the range of validity of the s-wave threshold law. Dunning and colleagues (Zollars *et al.* 1985; Dunning 1987) have carried out several careful studies of $k_{n\ell}$ at high $n \lesssim 100$, using different Rydberg atoms and relatively heavy particle collision energies with average values $\langle E_{rel} \rangle = 40$–$60$ meV. In the range $30 < n \lesssim 100$, they found $k_{n\ell}$ to be independent of n (and of ℓ) with an average value of $k_{n\ell} = (4 \cdot 2 \pm 1) \times 10^{-7}$ cm^3 s^{-1} (Dunning 1987); the constant value of $k_{n\ell}$ indicates that the Rydberg electrons attach with a cross

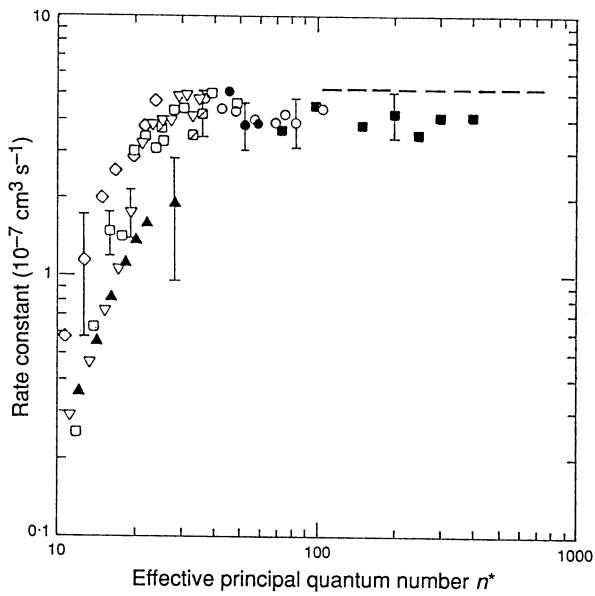

Fig. 9. Rate constants for Rydberg atom destruction (k_d) and for free ion production (k_i) in Rydberg atom collisions with SF_6 [taken from Ling *et al.* (1992) with permission]. ■: k_d—K(np) (Ling *et al.* 1992); ○: k_d—Rb(nd) (Zollars *et al.* 1985); ●: k_i—Rb(ns) (Zollars *et al.* 1985); ⫽ : k_i—Xe(nf) (Dunning 1987); □ : k_i—K(nd) (Dunning 1987); ▽: k_i—Na(np) (Beterov *et al.* 1987); ◇: k_i—Ne(ns) (Harth *et al.* 1989); ▲: k_i—Ne(nd) (Harth *et al.* 1989). The dashed line indicates the value of the limiting capture rate constant $k_c = 5 \cdot 15 \times 10^{-7}$ cm^3 s^{-1} (Vogt and Wannier 1954).

section $\sigma_e \sim 1/v \sim E^{-1/2}$ and therefore signals that the s-wave threshold region has been reached. Below about $n = 30$, $k_{n\ell}$ was observed to decrease by several groups (Zollars *et al.* 1986; Beterov *et al.* 1987; Harth *et al.* 1989; Kraft *et al.* 1989; Desfrancois *et al.* 1989). This behaviour is mainly due to the fact that an increasing number of ion pairs A^+–XY^-, formed in the primary electron transfer step, have insufficient kinetic energy to escape from the Coulomb field when n is lowered and thereby the ion pairs are created at smaller distances.

Very recently, Ling *et al.* (1992) extended the Rydberg electron attachment data for $XY = SF_6$, CCl_4 up to principal quantum numbers $n = 400$. Fig. 9 summarises the results of several groups over the range $10 < n \leq 400$. The rate constants k_{np}, measured by Ling *et al.* (1992) with $K(np)$ atoms from $n = 70$ to 400, are independent of n with an average value $\bar{k}_{np}$ $(n = 70\text{–}400) = (4\pm1)\times10^{-7}$ cm^3 s^{-1} and agree with the previous results of the Rice group in the range $30 < n \lesssim 100$. The limiting capture rate constant $k_c(SF_6) = 5\cdot15\times10^{-7}$ cm^3 s^{-1} of Vogt and Wannier (1954) is found to be compatible with the measured $\bar{k}_{np}$ within the experimental uncertainties. For comparison, we mention the results for $XY = CCl_4$ (i.e. formation of Cl^- ions by DA): Ling *et al.* (1992) report $\bar{k}_{np}$ $(n = 70\text{–}400) = (8\cdot5\pm2)\times10^{-7}$ cm^3 s^{-1}, and the capture rate constant $[\alpha(CCl_4) = 71\cdot7a_0^3$ (Yoshihara *et al.* 1980)] is calculated to be $k_c(CCl_4) = 6\cdot57\times10^{-7}$ cm^3 s^{-1}. While the values of k_c scale as the square root of the polarisability, favouring CCl_4 by a factor of 1·275, the measured Rydberg attachment rate constants differ by a factor of about 2. It will be interesting to see a comparison between SF_6 and CCl_4 threshold attachment involving free electrons in the future.

For purposes of comparison, it is of interest to derive from the Rydberg rate constants $k_{n\ell}$ the velocity-averaged free electron attachment cross sections $\bar{\sigma}_e$. Dunning (1987) presented cross sections $\bar{\sigma}_e(E)$ for several molecules obtained with the simple relation

$$\bar{\sigma}_e = k_{n\ell}/v_{rms}\,, \tag{14}$$

where v_{rms} is the root-mean-square velocity of the Rydberg electron and the associated kinetic energy is given by $\langle E\rangle_{n\ell} = mv_{rms}^2/2 = |E_{n\ell}|$. Relation (14) was also used by Chutjian and Alajajian (1985) to compare their free electron cross sections with the available Rydberg data. Instead of (14), Ling *et al.* (1992) used the relation

$$\bar{\sigma}_e = k_{n\ell}/v_m\,, \tag{15}$$

replacing the root-mean-square velocity by the median velocity v_m of the electrons attached, i.e. the Rydberg electron velocity such that integration of the expression for the Rydberg rate constant (see equation 9) from 0 to v_m,

$$\int_0^{v_m} v\sigma_e(v)\, g_{n\ell}(v)\, dv \;\equiv\; k_{n\ell}/2\,, \tag{16}$$

yields a value one half that for integration from 0 to ∞. The values of $\bar{\sigma}_e$ so obtained are positioned on the electron energy axis according to the value $E_m = mv_m^2/2$. Note that the values of the median velocity v_m and of the median energy E_m differ substantially from the respective values for the root-mean-square

velocity $v_{\rm rms}$ and the average kinetic energy $\langle E \rangle_{n\ell}$; e.g. at $n = 400$, one has $E_{\rm m} = 10$ μeV (Ling *et al.* 1992) as compared with $\langle E \rangle_{n\ell} = 85$ μeV. Whether the use of (15) is more appropriate than that of (14) can only be decided through an intercomparison of precise Rydberg rate constants $k_{n\ell}$ (measured from medium to very high n at sufficiently large heavy particle collision energies) with accurate free electron cross sections (see also the discussion in Section 3*c* in connection with Fig. 12).

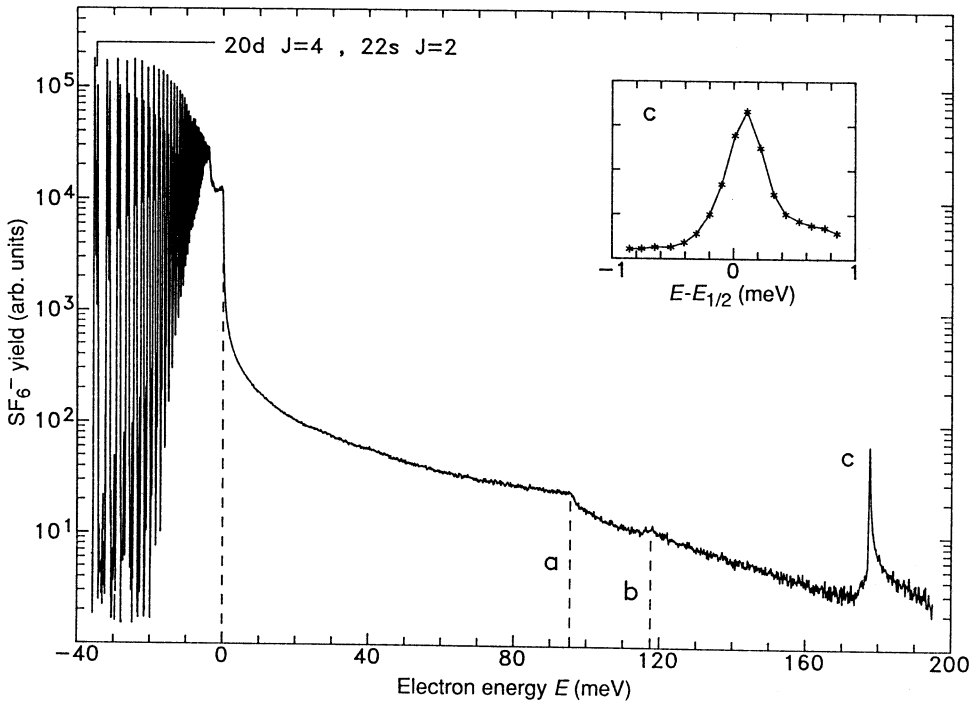

Fig. 10. SF_6^- yield in collisions of $Ar^{**}(ns, nd)$ Rydberg atoms ($E < 0$) and of free electrons ($E > 0$) with SF_6 molecules ($T = 300$ K), as measured in the present work with a photon energy bandwidth of 0·15 meV (FWHM). In the range $0 < E < 175$ meV, the SF_6^- yield is proportional to the electron attachment cross section for formation of SF_6^- ions with average lifetimes around 80 μs (see also text). The downward step (a) occurs at the threshold for excitation of one quantum of the ν_1 vibration in SF_6. The structure (b) is located at the onset of ν_3 vibrational excitation. The sharp peak (c) corresponds to SF_6^- formation by very slow electrons associated with the $Ar^+(^2P_{1/2})$ threshold; the peak has a width of 0·4 meV (FWHM), see inset, indicating an overall resolution of 0·2 meV or better (see text).

(3c) Attachment of Free Electrons to SF_6 at Sub-meV Resolution

Now we discuss our free electron attachment data, obtained for $XY = SF_6$ with sub-meV resolution and reported in part in a recent publication (Klar *et al.* 1992). Fig. 10 surveys the SF_6^- yield, measured in the electron energy range $(-40, +200)$ meV with $\Delta E = 0{\cdot}15$ meV optical resolution. Negative energies are equivalent to electron binding energies in the Ar^{**} Rydberg atoms, excited from $Ar^*(4p\,^3D_3)$ by the second laser at a wavelength longer than 462 nm. The data have been corrected for the wavelength dependence of the photon flux and of the

photoionisation cross section. The relative energy scale is established with an accuracy of about 10^{-3} by frequency markers from a calibrated fused-silica etalon with a free spectral range of 199·5 GHz (at 466 nm) and a finesse around 20. The absolute energy scale is determined on the basis of the well-known energy levels for $Ar^{**}(n\mathrm{s}, J{=}2)$ and $Ar^{**}(n\mathrm{d}, J{=}4)$ (Kraft 1991).

The sharp drop in the SF_6^- yield at zero energy corresponds to the transition from Rydberg atom collisions to free electron collisions; it mainly reflects the fact that the density of free electrons scales as $E^{-1/2}$ for $E > 0$, while the density of Rydberg atoms excited at very high n is practically constant. Note that the yield Y (ions per second) for SF_6^- production in $Ar^{**}(n\ell)$+SF_6 collisions is given by

$$Y_{n\ell} = n(\mathrm{SF_6}) n_{n\ell}\, k_{n\ell}\, V_{n\ell}\,, \tag{17}$$

while that due to free electron attachment reads

$$Y_e = n(\mathrm{SF_6})\, n_\mathrm{e}(E)\, k_\mathrm{e}(E) V_\mathrm{e} = n(\mathrm{SF_6}) j_\mathrm{e}\, \sigma_\mathrm{e}(E)\, V_\mathrm{e}\,; \tag{18}$$

$n(\mathrm{SF_6})$, $n_{n\ell}$ and $n_\mathrm{e}(E)$ are the respective (average) densities of the (diffuse) SF_6 target, the $Ar^{**}(n\ell)$ Rydberg atoms, and the free electrons; $V_{n\ell}$ and V_e are the corresponding effective collision volumes, from which SF_6^- ions are detected; $j_\mathrm{e} = n_\mathrm{e}\, v$ is the constant free electron flux density (normalisation to photoionisation cross section!).

For a given target density, $Y_{n\ell}$ is essentially constant at high n, because the quantities $n_{n\ell}$, $k_{n\ell}$ and $V_{n\ell}$ do not change significantly for $n \gtrsim 70$. The step at $E = -4$ meV can be attributed to a decrease in $n_{n\ell}$, associated with removal of the reactive $Ar^{**}(n\ell)$ flux by field ionisation in the pulsed ion drawout field ($23\,\mathrm{V\,cm^{-1}}$). Close to threshold, k_e is nearly constant, and Y_e varies mainly according to the energy dependence of $n_\mathrm{e}(E) \sim v^{-1} \sim E^{-1/2}$; expressed differently, Y_e reflects the threshold behaviour of the attachment cross section, since $n_\mathrm{e}\, k_\mathrm{e} = (j_\mathrm{e}/v)(\sigma_\mathrm{e}\, v) = j_\mathrm{e}\, \sigma_\mathrm{e} = \mathrm{const.}\, \sigma_\mathrm{e}$.

In the absence of stray electric fields, the minimum free electron energy is about 1 μeV, corresponding to a laboratory electron velocity identical to the Ar^* velocity ($560\,\mathrm{m\,s^{-1}}$). The presence of stray fields will modify the $E^{-1/2}$ dependence of $n_\mathrm{e}(E)$ near threshold, as referred to the photon energy scale, and will limit the useful free electron data range towards lower energies. We shall assess this problem in more detail below in simulations of the threshold behaviour.

Let us return to the discussion of Fig. 10. As explained above, the SF_6^- yield for $E > 0$ is proportional to the free electron attachment cross section $\sigma_\mathrm{e}(E)$; in the range 1 to 95 meV, it decreases by a factor of about 30, i.e. more rapidly than given by the s-wave behaviour. At $E = 95{\cdot}4$ meV, it shows a sharp cusp (downward step) associated with the opening of a new inelastic channel, namely that for excitation of one quantum of the ν_1 symmetric stretch vibration in SF_6. Such structure has been theoretically predicted to occur in the e^-–SF_6 attachment cross section by Gauyacq and Herzenberg (1984). Around $E = 117$ meV (onset of ν_3 vibrational threshold) there are hints of a weak upward cusp. We note that electron scattering studies of SF_6 (Rohr 1977; Randell *et al.* 1992) exhibit prominent threshold peaks associated with the onsets for ν_1 and ν_3 vibrational excitation. These processes compete with electron attachment and thereby cause structure in the attachment cross section in a way that depends on the coupling strength.

Another prominent feature occurs near $E = 177{\cdot}5$ meV, the position of the $Ar^+(^2P_{1/2})$ photoionisation threshold. A sharp peak (FWHM 0·4 meV) with a tail to higher energies is observed, which is due to threshold attachment of slow electrons, formed in the process

$$Ar^*(4p\,^3D_3) + \gamma_2(\lambda_2 \leq 433{\cdot}3\ \text{nm}) \longrightarrow Ar^+(^2P_{1/2}) + e^- . \qquad (19)$$

The size of this threshold peak allows the derivation of the probability of process (19) relative to threshold photoionisation to the $Ar^+(^2P_{3/2})$ fine structure state as about 1%. The width of this peak presents a direct measure of the energy resolution in the experiment of Fig. 10. Convolution of an s-wave threshold cross section $\sigma_e(E) \sim E^{-1/2}$ with a Gaussian resolution function of width ΔE_G (FWHM) results in a broadened threshold peak ΔE_T with a full width half maximum of $2{\times}\Delta E_G$. From the measured value $\Delta E_T = 0{\cdot}4$ meV, we obtain $\Delta E_G = 0{\cdot}2$ meV. In view of the Gaussian photon bandwidth $\Delta E_p = 0{\cdot}15$ meV, we conclude that the influence of stray electric fields on the resolution is below 0·1 meV. From simulations of the attachment cross section, measured at the $Ar^+(^2P_{3/2})$ threshold, we come to the same conclusion, namely that the overall energy resolution was 0·2 meV or better.

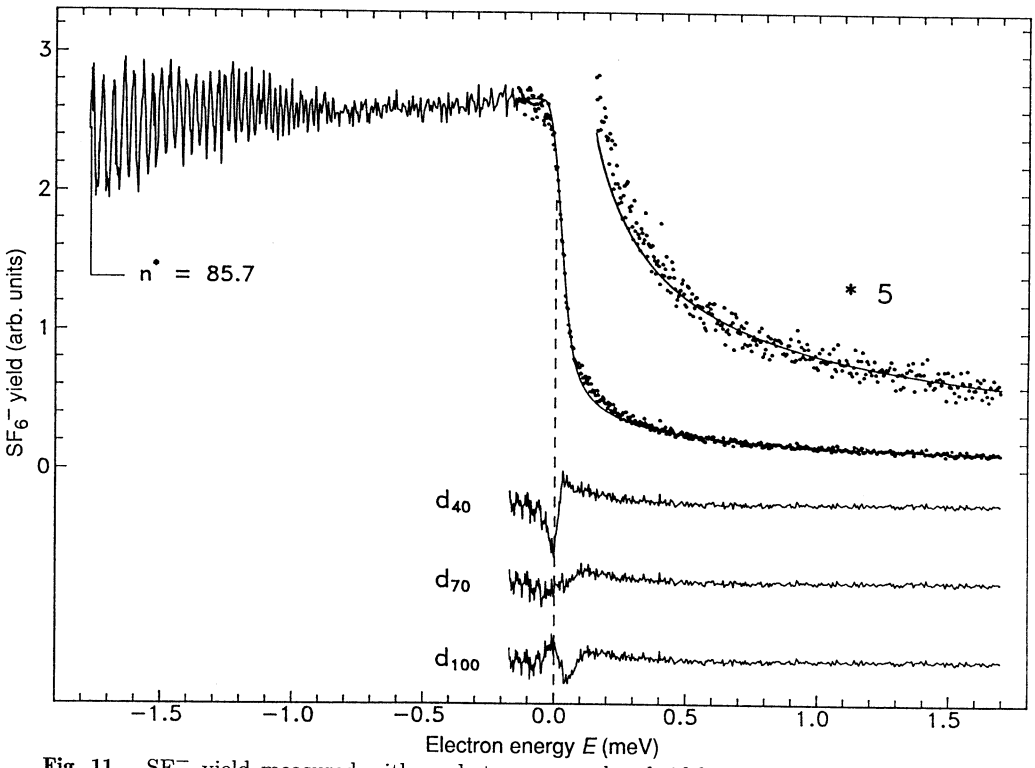

Fig. 11. SF_6^- yield measured with a photon energy bandwidth of 40 μeV (FWHM) in the energy range $(-1{\cdot}8, +1{\cdot}7)$ meV. The data are compared with model cross sections, convoluted with Gaussian functions of 40, 70 and 100 μeV (FWHM) to simulate the overall energy resolution. The quantities d_{40}, d_{70} and d_{100} correspond to the respective differences between the measured and the calculated yields. The smooth curve through the data points represents the calculation for a resolution of 70 μeV.

In order to obtain more detailed information on the near-threshold region, we carried out experiments with a photon bandwidth of 40 μeV (FWHM, lineshape not far from Gaussian) over a limited energy range ($-1{\cdot}8$ to $+1{\cdot}7$ meV) around the $Ar^+(^2P_{3/2})$ threshold. The corresponding SF_6^- yield is shown in Fig. 11. For comparison with the experimental data we carried out simulation calculations of the ion yield using the following analytical cross section function:

$$\sigma(E) = \begin{cases} \sigma_0 = \text{const.} & E < 0, \text{ Rydberg atom collisions} \quad (20a) \\ (\sigma_1/E)[1-\exp(-\beta E^{1/2})] & E > 0, \text{ free electron collisions.} \quad (20b) \end{cases}$$

The expression for the free electron cross section possesses the same functional form that was suggested some time ago by Klots (1976):

$$\sigma_K(E) = (\pi a_0^2/2E)\{1 - \exp[-4(2\alpha E)^{1/2}]\}. \quad (21)$$

For $E \to 0$, $\sigma_K(E)$ agrees with the capture cross section $\sigma_c(E)$ in (6) and interpolates to the de Broglie s-wave cross section $\pi\lambda^2 = \pi {a_0}^2/2E$ at higher energies. Compared with the measured energy dependence of the attachment yield, the cross section $\sigma_K(E)$ decreases too slowly with rising E (see also Klar *et al.* 1992), but we found that the related form (20b) with an adjusted exponential factor β provides an excellent fit to our data over the range 1–95 meV (see Fig. 12). With E given in meV, β is fixed at $0{\cdot}405$ (note that β was not treated as a fit parameter in the simulation of the threshold behaviour in Fig. 11). The parameters σ_0 and σ_1 in (20a) and (20b) are fixed through the measured yields in the ranges $(-0{\cdot}2, -0{\cdot}1)$ meV and $(+1{\cdot}0, +1{\cdot}7)$ meV. In this way the cross section function $\sigma(E)$ is fully predetermined; the zero point of the energy scale was treated as a free parameter (note that the fitted zero point is an effective value, which incorporates the suppression ΔE_F from the 'true zero' due to stray electric fields).

The real problem in the simulation is the effective energy spread function $S(E)$, which should properly incorporate the broadening effects due to the photon bandwidth, the Doppler effect, and potential gradients across the effective volume for attachment reactions. For demonstration purposes it is sufficient to simply use Gaussian functions for $S(E)$ with different widths ΔS (FWHM). In Fig. 11, the smooth curve corresponds to the simulated yield, obtained by convolution of the predetermined cross section $\sigma(E)$ with a Gaussian $S(E)$ of $\Delta S = 70$ μeV. In the lower part of Fig. 11, the differences $d_{\Delta S}$ between the experimental data and the simulated yield functions are shown for widths $\Delta S = 40$, 70 and 100 μeV. The choice $\Delta S = 70$ μeV results in the best overall agreement; although some deviations between the data and the simulated yield remain, we consider this agreement as very satisfactory in view of the simple choice for the function $S(E)$. From the results in Fig. 11 we conclude that the effective resolution of the experiment was better than 100 μeV (FWHM) and probably close to 70 μeV. From the fit calculations, the zero point is determined to within ± 15 μeV.

The partial resolution of Rydberg structure in Fig. 11 at energies $-1{\cdot}7$ to $-1{\cdot}2$ meV allows us to estimate the suppression of the threshold as $\Delta E_F = 80 \pm 20$ μeV. Using the classical relation (10) one estimates the corresponding stray electric field to be $F \approx 1{\cdot}1$ mV mm^{-1}, a value much too high to be compatible with the effective resolution of our attachment experiments. As an alternative to

(10) we suggest estimating F from the energy value E_F below the true ionisation limit, at which discrete Rydberg excitations start to disappear (Harmin 1984; Neukammer *et al.* 1987; Ling *et al.* 1992),

$$F\ (\mathrm{mV\,mm^{-1}}) = 8{\cdot}2[E_F\ (\mathrm{meV})]^{5/2}, \tag{22}$$

and then identifying the energy E_F with the shift ΔE_F. From $E_F = 80\ \mu$eV, we obtain for the stray electric field $F = 15\ \mu\mathrm{V\,mm^{-1}}$, a value which seems much more realistic than the number estimated from (10). We conclude the discussion of Fig. 11 by stating that stray electric fields contribute to the finite energy resolution of our attachment experiments at about the 60 μeV (FWHM) level and that the value of F is likely to be around 40 $\mu\mathrm{V\,mm^{-1}}$ (or less).

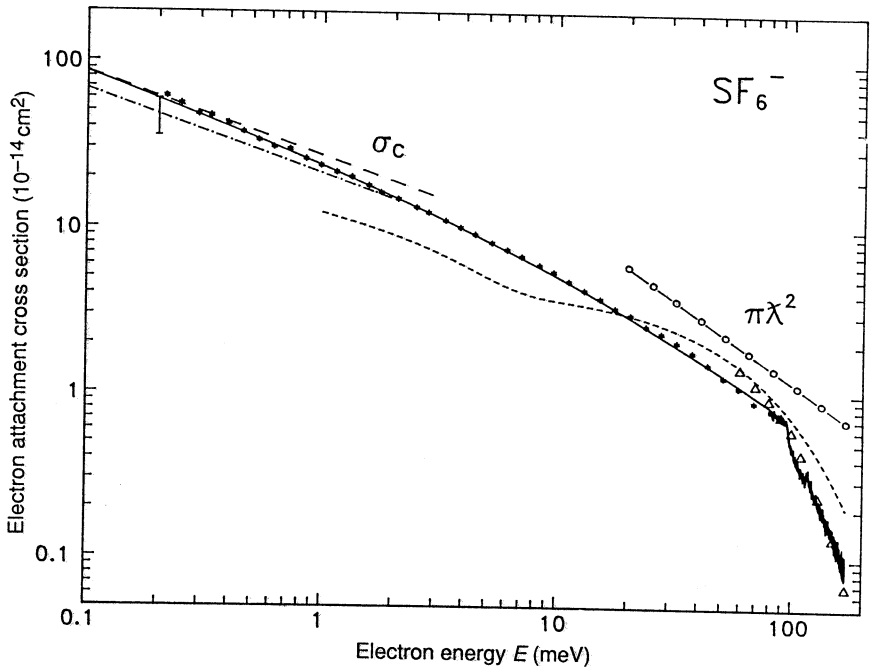

Fig. 12. Absolute cross section for attachment of free electrons to SF_6 in the energy range 0·1–200 meV: average data points (stars, 0·2–80 meV) and original data points (85–170 meV), present LPA results; smooth line (0·1–80 meV), fit to our data points (see equation 23); short-dash line, TPSA cross section equation (11) (Chutjian and Alajajian 1985); triangles, swarm-derived cross section (Hunter *et al.* 1989); dash–dot line, cross section (26) derived from Rydberg atom collisions at high n (Ling *et al.* 1992); long-dash line, s-wave capture cross section σ_c for polarisation potential (Vogt and Wannier 1954), equation (25).

From the data in Figs 10 and 11, we generated a set of absolute cross sections $\sigma_e(E)$ for attachment of free electrons to SF_6 in the energy range 0·2–175 meV by normalisation of our relative cross sections to the accurate $T = 300$ K attachment rate constant $k_e(T{=}300\ \mathrm{K}) = 2{\cdot}27(9){\times}10^{-7}\ \mathrm{cm^3\,s^{-1}}$ of Petrović and Crompton (1985), using (12) and (13). These absolute cross sections are shown in Fig. 12 and compared with the cross section derived by Chutjian and Alajajian (1985) from their TPSA data (see equation 11), with the high n Rydberg electron attachment cross section curve $\bar{\sigma}_e(E_m)$ of Ling *et al.* (1992), and with the swarm-derived cross sections of Hunter *et al.* (1989). The smooth curve through

our data points in the range 0·1–85 meV represents a fitted cross section of functional form (20b) (E in meV):

$$\sigma_{\rm fit}(E) = (7130 \times 10^{-16}\ {\rm cm}^2/E) \times [1 - \exp(-0{\cdot}405\ E^{1/2})]\,. \tag{23}$$

The parameters β and σ_1 have estimated uncertainties of $\Delta\beta/\beta \approx \pm 10\%$ and $\Delta\sigma_1/\sigma_1 \approx \pm 5\%$. At very low energies this model fit cross section $\sigma_{\rm fit}(E)$ displays the $E^{-1/2}$ behaviour in the form (E in meV)

$$\sigma_{\rm fit}(E \to 0) = (2888 \pm 400) \times 10^{-16}\ {\rm cm}^2/E^{1/2}\,, \tag{24}$$

in very good agreement with the limiting electron capture cross section of Vogt and Wannier (1954), which for SF_6 is given by (E in meV)

$$\sigma_{\rm c}(E \to 0) = 2726 \times 10^{-16}\ {\rm cm}^2/E^{1/2}\,. \tag{25}$$

In the units of equations (23)–(25), the Rydberg collision-derived cross section $\bar{\sigma}_{\rm e}$ is given by

$$\bar{\sigma}_{\rm e}(E) = (2133 \pm 533) \times 10^{-16}\ {\rm cm}^2/E^{1/2}\,. \tag{26}$$

If E is interpreted as the median Rydberg electron energy $E_{\rm m}$, equation (26) describes the attachment cross section in the range 0·01–2 meV (see Ling *et al.* 1992, Fig. 7). Within the mutual uncertainties the experimental results represented by equations (23), (24) and (26) show satisfactory agreement.

We stress that the limiting s-wave behaviour of the attachment cross section is only reached at sub-meV energies. Our measured relative cross sections leave no doubt that at energies $\gtrsim$0·5 meV the attachment cross section decreases more rapidly with rising energy than a $E^{-1/2}$ function. At $E = 1$ meV, for example, the value calculated from (23) is 18% lower than expected from the limiting cross section (24). These deviations from the $E^{-1/2}$ behaviour should in principle also be visible in the Rydberg atom collision data through a weak increase of $k_{n\ell}$ from $n = 35$ to 400, but the scatter of the experimental data in Fig. 9 (note that each point represents an *absolute* measurement of the respective rate constant) is too large to draw conclusions in this direction. Our high resolution data in Fig. 11 exhibit a weak increase of the SF_6^- yield within the Rydberg energy range $(-1{\cdot}8, -0{\cdot}1)$ meV towards very high n; so far, we have not carried out separate tests of the Rydberg excitation probability in this range, but we expect that it is essentially constant in view of the behaviour of the photoionisation cross section close to the $Ar^+(^2P_{3/2})$ threshold (Fig. 4) and of the smooth tuning characteristics of the etalon-narrowed multimode ionisation laser (mode spacing about 40 MHz). Therefore, the increase in the SF_6^- yield towards $E = 0$ may—at least in part—be associated with a rise of $k_{n\ell}$ with n. In this connection it will be interesting to see the results of calculations for $k_{n\ell}$ presently being carried out by the Rice group (Dunning, personal communication 1992) on the basis of equation (9) with our free electron cross sections. These calculations may also shed light on the question of whether the choice of the median velocity and energy (equations 14 and 16) in deriving $\bar{\sigma}_{\rm e}(E)$ functions from $k_{n\ell}$ data is appropriate.

Let us now discuss the cross sections at energies above 1 meV (Fig. 12). One notes significant differences between the TPSA-derived cross section (11) and our LPA cross sections. Below $E \approx 20$ meV the TPSA cross sections are lower and above they are higher than our results such that the thermal rate constants $k_e(T{=}300\text{ K})$ for the two data sets agree according to their common normalisation. These differences are also clearly observed in Fig. 8 in which both the TPSA (dashed curve) and our LPA yield (smooth curve) are compared after convolution of the respective cross sections (equation 11 for TPSA) with a Gaussian resolution function of 8 meV width (FWHM). We attribute the differences between the TPSA data and our results to be mainly due to an effective discrimination in the TPSA measurements against attachment processes at low electron energies and suggest them to be associated with the dc electric field, present for the extraction of the product ions (Chutjian and Alajajian 1985; Alajajian *et al.* 1988).

At energies above 60 meV the swarm-derived cross sections of Hunter *et al.* (1989), which were synthesised to join the TPSA cross sections at lower energies, show satisfactory agreement with our data. This agreement is of special interest in connection with an aspect so far omitted from the discussion, namely the lifetime of the SF_6^- ions formed by attachment of free electrons as a function of electron energy E. Before we dwell on this point in some depth, we mention that in the energy range considered ($E < 175$ meV) the only significant negative product ions which we observe are SF_6^- ions. The ratio of the SF_5^- to the SF_6^- signals was found to be $<10^{-3}$ in selected Rydberg atom experiments ($n = 18, 28, 43$) and for attachment of free electrons at $E \approx 1$ meV. At $E \approx 170$ meV the SF_5^- fraction was below 10% (i.e. lower than the fractions reported by Hunter *et al.* 1989).

An important point with regard to the overall energy dependence of the measured cross section for SF_6^- formation is the lifetime of the SF_6^- ions, which will in general depend on the energy of the attached electron. So far, no measurements of lifetimes for free SF_6^- ions produced by monoenergetic free electrons in the range 0–200 meV exist, although data involving SF_6^- formation by attachment of non-monoenergetic electrons or of Rydberg electrons were reported with conflicting results (see e.g. Christophorou 1978; Astruc *et al.* 1983; Brincourt *et al.* 1989 and references in these papers). We note that results for Rydberg electron attachment at high principal quantum numbers ($n \gtrsim 30$), i.e. in the region of validity of the (quasi) free electron model, have shown through the identity of the A^+ and SF_6^- signals (Dunning 1987; Harth *et al.* 1989) that the autodetachment lifetimes of the corresponding SF_6^- ions are around 0·5 ms or longer. These findings also demonstrate that the electric fields encountered by the SF_6^- ions after their formation until detection do not lead to significant losses by field detachment. These high n Rydberg results are expected to be equally valid for SF_6^- ions formed in collisions with free electrons at low energies (<10 meV). With rising electron energy the SF_6^- lifetime will in general decrease (see e.g. Klots 1976; Christophorou 1978), and thereby the measured cross sections could be smaller than the cross sections for the primary attachment process, especially at higher energies (above the ν_1 vibrational threshold $E = 95{\cdot}4$ meV).

In separate experiments we recently measured the time-of-flight (TOF) distribution of SF_6^- ions, formed in collisions with $Ar^{**}(30d, J{=}4)$ atoms; for this purpose the repetition rate of Laser 1 (see Fig. 6) was reduced to about 5·5 kHz, while all the other experimental parameters were kept as usual. A

rather broad TOF distribution with enhanced intensities around 50 and 100 μs and with an average time between the formation and the detection of the SF_6^- ions close to 80 μs was observed. This peculiar TOF distribution reflects the special experimental conditions of the timing sequence in combination with the ion lens system (Fig. 5) and the ion deflection and detection system behind the quadrupole mass spectrometer. Regarding the comparison of our LPA data with the TPSA results, we note that the detection time of the SF_6^- ions in the TPSA work amounted to about 75 μs (Chutjian, personal communication 1992) and was therefore similar to the one in our experiment.

As mentioned above, the cross sections derived from swarm experiments (Hunter *et al.* 1989), in which collisions with the buffer gas may stabilise the SF_6^- ions, agree quite well with our values in the range 60–175 meV, indicating that no major losses of SF_6^- ions due to possibly reduced lifetime occur in the investigated energy range. It would nevertheless be worthwhile to carry out a high resolution attachment experiment with a setup which allows mass-resolved ion sampling at several different, well-defined detection times.

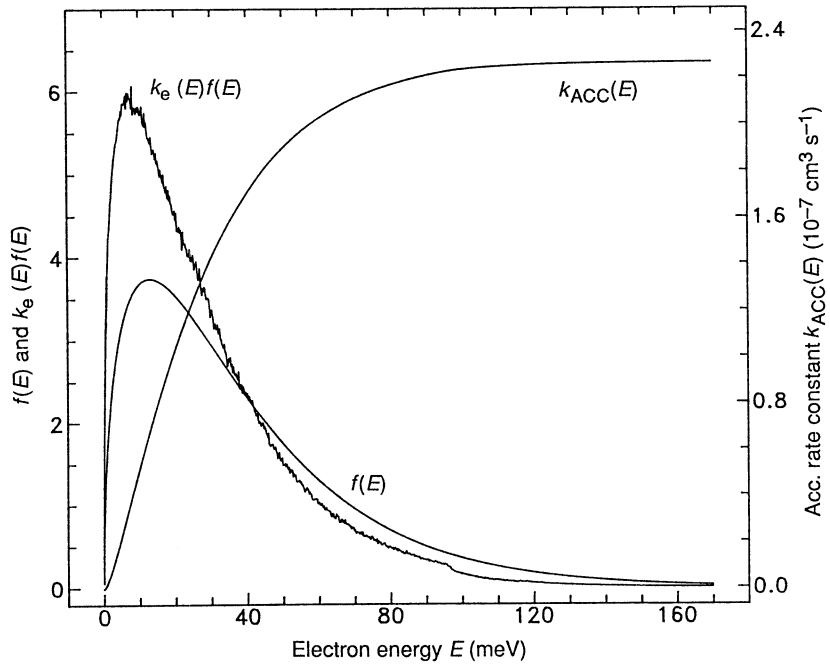

Fig. 13. Illustration of the energy-dependent contributions to the average rate constant for electron attachment at $T = 300$ K (see text): $f(E)$ is the electron distribution function at $T = 300$ K (in $0{\cdot}005$ meV^{-1}); $k_e(E)f(E)$ is in 10^{-9} cm^3 s^{-1} meV^{-1}; and $k_{ACC}(E)$ is the contribution to the rate constant accumulated in the energy range $(0, E)$.

As already explained, the absolute scale for our LPA cross sections shown in Fig. 12 was obtained by normalisation of the average rate constant, calculated for an SF_6 target and electron energy distribution at a temperature of $T = 300$ K with our relative cross sections, to the value $k_e(T{=}300\text{ K}){=}2{\cdot}27(9){\times}10^{-7}$ cm^3 s^{-1}, measured by Petrović and Crompton (1985) with the Cavalleri swarm technique.

Fig. 13 demonstrates that our data extend over a sufficiently large energy range to guarantee 'saturation' of the accumulated rate constant

$$k_{\mathrm{ACC}}(E) = \int_0^E k_{\mathrm{e}}(E')\, f(E')\, \mathrm{d}E' \tag{27}$$

at higher energies. At $E = 22{\cdot}3$ meV, $k_{\mathrm{ACC}}(E)$ amounts to 50% of the full value.

As shown above, contributions from other product ions (SF_5^-) are negligible at energies $\lesssim$175 meV. The exponential decay of the distribution function $f(E)$ efficiently suppresses any contributions due to SF_5^- ions at energies above 175 meV, such that they introduce uncertainties in the normalisation of the rate constant well below 1%. With the $\pm$4% uncertainty quoted by Petrović and Crompton (1985) for their measured $T = 300$ K rate constant, we assign a total uncertainty of $\pm$5% to our absolute cross sections as a result of the normalisation procedure. We estimate that other possible sources of systematic error, discussed in Section 2, amount to an additional uncertainty below 10% and well below 5% over limited energy ranges.

One of the prominent features in the energy-dependent cross section and rate constant is the sharp downward step, which occurs precisely (to within $\pm 0{\cdot}2$ meV) at the threshold for the excitation of one quantum of the symmetric stretch vibration ν_1 of SF_6 [$E(\nu_1) = 95{\cdot}4$ meV]. This structure has been observed here for the first time, corroborating the theoretical prediction by Gauyacq and Herzenberg (1984). These authors discussed the attachment of very slow electrons to polyatomic molecules with a model in which the s-wave of the incident electron dominates and the mechanism of capture is a non-adiabatic coupling due to the velocities of the nuclei; the non-adiabatic coupling enables the s-wave electron to make a direct transition into the bound state from states of positive energy, without the intervention of a temporary trapped state of positive energy (as is often present for $L > 0$ in the form of shape resonances). Gauyacq and Herzenberg (1984) assumed that the initial stage of the distortion of the nuclear framework is through a breathing mode, described by a single coordinate R and compatible with a perturbation of spherical symmetry associated with the s-wave electron. Subsequently, a nuclear wave propagates outwards along R, the extra electron being loosely attached. For SF_6^-, dissociative channels are not available at the energies of interest here, and the long lifetime of the SF_6^{-*} ion is attributed to a redistribution of the available energy over all the nuclei in a chaotic state before the nuclear framework can oscillate back to its initial configuration (Gauyacq and Herzenberg 1984). Possibly the attachment process is supported by a virtual state, which enhances the amplitude of the s-wave electron at the molecule. Gauyacq and Herzenberg carried out calculations of the attachment cross sections, assuming model potentials for the negative ion product energy $E_0^-(R)$ around the equilibrium distance R_0 in the neutral SF_6 molecule and equating the frequency of the breathing distortion to the frequency of the symmetric stretch vibration ν_1 in SF_6. Obviously, the attachment process and the inelastic scattering channels, corresponding to $\nu_1, 2\nu_1$, ... excitation, are strongly coupled in this model, and the calculated attachment cross sections yielded prominent, rounded downward steps at the opening of each new channel (Gauyacq and Herzenberg 1984, Fig. 4).

In Fig. 14 we compare our experimental rate constant $k_{\mathrm{e}}(E)$ with those two results of the model calculations of Gauyacq and Herzenberg (1984) which are

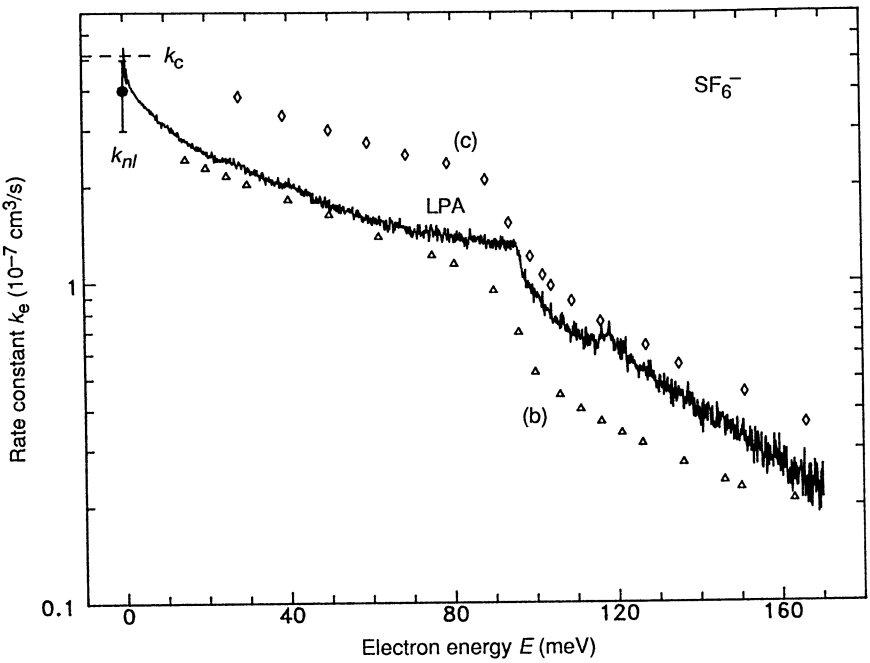

Fig. 14. Comparison of experimental (LPA) rate constants $k_e(E)$ (full curve) with the theoretical results of Gauyacq and Herzenberg (1984): Δ, case (b); ◇, case (c) (see text). The dashed line is the capture rate constant $k_c = 5{\cdot}15\times10^{-7}$ cm^3 s^{-1} (Vogt and Wannier 1954); the point with the error bars is the high n Rydberg rate constant (Ling *et al.* 1992).

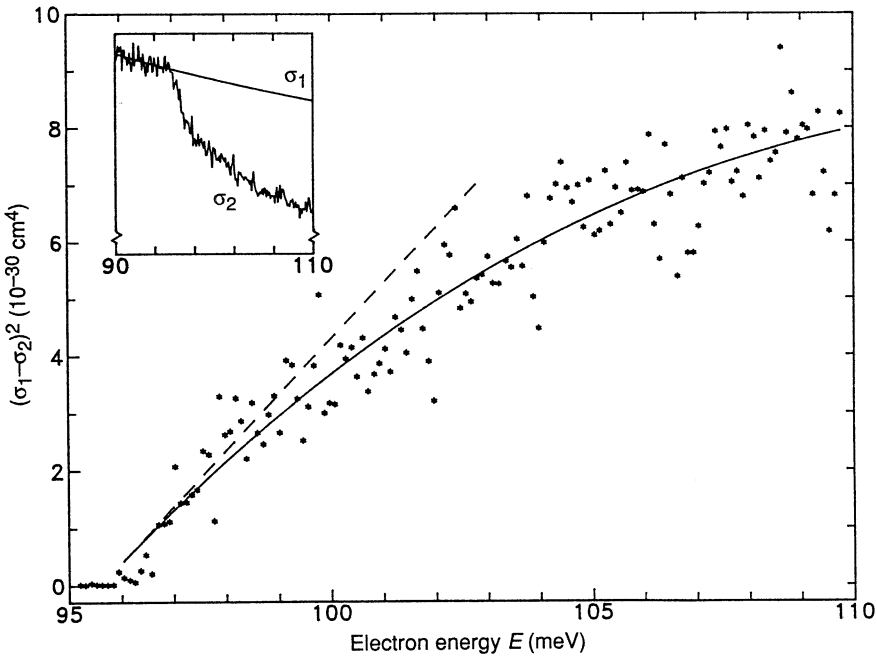

Fig. 15. Energy dependence of the downward step in the SF_6^- attachment cross section above the ν_1 vibrational threshold [$E(\nu_1) = 95{\cdot}4$ meV]: the square of the difference cross section $(\sigma_1-\sigma_2)^2$ is plotted versus electron energy.

closest to experiment and were labelled case (b) (triangles) and case (c) (diamonds) in their paper. Case (c) corresponds to a potential $E_0^-(R)$, which agrees with that of the harmonic oscillator potential $E_0(R)$ of the neutral molecule for $R \leq R_0$ and bends downward for $R > R_0$ with horizontal slope at R_0 (i.e. the stabilisation radius R_s equals R_0); this case yields the largest attachment rate constant with an average value at $T = 300$ K of $k_e^c(T{=}300\text{ K}) = 4{\cdot}14{\times}10^{-7}$ cm^3 s^{-1}. In case (b) the stabilisation point R_s is slightly below R_0 and $E_0^-(R)$ is bound relative to $E_0(R)$ at $R = R_0$; the thermal rate constant comes out as $k_e^b(T{=}300\text{ K}) = 1{\cdot}96{\times}10^{-7}$ cm^3 s^{-1}. The overall energy dependence of the calculated rate constants $k_e^b(E)$, $k_e^c(E)$ is in good qualitative agreement with experiment for both case (b) and case (c); $k_e^b(E)$ and $k_e^c(E)$ are smaller and larger, respectively, than the measured $k_e(E)$ at all energies.

As mentioned above and observed in Fig. 14, the theoretical rate constants show a rounded step at the ν_1 vibrational onset [$E(\nu_1) = 95{\cdot}4$ meV]. In contrast the experimental rate constant $k_e(E)$ exhibits a more or less abrupt change of slope at $E(\nu_1)$. Note that the energy resolution near 95 meV is limited to about 0·6 meV by the Doppler effect (see Section 2). In order to characterise the behaviour of the observed downward step in a more quantitative way we plot the square of the difference between the extrapolated cross section σ_1 and the measured cross section σ_2 as a function of electron energy E in Fig. 15. Since the attachment channel and the inelastic channel are both mediated by the s-wave, one may expect the leading term to behave as

$$(\sigma_1 - \sigma_2)^2 \sim E - E(\nu_1)\,, \tag{28}$$

i.e. a straight line, as indicated by the dashed line in Fig. 15. The smooth curve in Fig. 15 represents a fit to the experimental squared difference $(\sigma_1{-}\sigma_2)^2$, using the expression

$$(\sigma_1 - \sigma_2) = a_1[E - E(\nu_1)]^{1/2} + a_2[E - E(\nu_1)]^{3/2}\,, \tag{29}$$

with $a_1 = 9{\cdot}88{\times}10^{-16}$ cm^2(meV)$^{-1/2}$ and $a_2 = -0{\cdot}17{\times}10^{-16}$ cm^2(meV)$^{-3/2}$. The deviations from straight-line behaviour are substantial, as might have been expected in view of the strong polarisation interaction for the $e^-{+}SF_6$ system [at $r = 10a_0$ for example the polarisation potential equation (5) with $\alpha = 44{\cdot}1a_0^3$ offers an attraction of 60 meV]. We mention that the role of the polarisation potential in connection with the threshold behaviour of cross sections has been discussed previously in some detail for photodetachment processes (e.g. O'Malley 1965; Hotop *et al.* 1973; Hotop and Lineberger 1973).

An interesting question in connection with the downward step is associated with the problem of the lifetime for the SF_6^- ions as a function of electron energy across the ν_1 threshold. This aspect was not taken into account in the theoretical calculations. It is possible that the lifetime decreases at $E(\nu_1)$ with the consequence that the magnitude of the downward step depends on the detection time of the SF_6^- ions.

4. Summary and Outlook

In this paper, we have presented a selective discussion of electron attachment to molecules at low energies with emphasis on threshold phenomena, as investigated

with sub-meV resolution for SF_6. At energies below 1 meV the attachment cross section reaches the behaviour expected for s-wave capture ($\sigma_e \sim E^{-1/2}$) with good agreement between the free electron LPA results (Klar *et al.* 1992), the Rydberg electron data at high principal quantum numbers n (Ling *et al.* 1992) and the theoretical cross section (Vogt and Wannier 1954) for electron capture through the e^-–SF_6 polarisation potential. The LPA data reveal substantial coupling of the electron attachment process with vibrationally inelastic scattering channels, especially at the $SF_6(\nu_1)$ threshold ($E = 95{\cdot}4$ meV), in agreement with the theoretical predictions of Gauyacq and Herzenberg (1984).

Application of the LPA method with sub-meV resolution to other molecules such as F_2, HI and CCl_4 should provide detailed and improved insight into threshold attachment phenomena. Moreover, we are working on an extension of the method in order to investigate the attachment of monoenergetic electrons to clusters in a supersonic target beam. Several molecular clusters exhibit an interesting 'zero energy resonance', not present in the attachment to the monomer (Märk 1991 and referencs therein) and not studied with high resolution so far. Recent data on electron transfer from state-selected rare gas Rydberg atoms to N_2O clusters have revealed an intriguing dependence of the negative cluster ion spectra on principal quantum number (Kraft *et al.* 1990), corresponding to size-selective negative cluster ion formation at very low electron energies ($\lesssim$10 meV). Clearly, attachment spectroscopy with monoenergetic electrons holds the promise of a lively and interesting future.

Acknowledgments

Our LPA work has been supported by the Deutsche Forschungsgemeinschaft through Sonderforschungsbereich 91. We are indebted to L. G. Christophorou, F. B. Dunning and E. Illenberger for permission to use figures from their work, as reproduced in Figs 1, 7 and 9 of this paper. We gratefully acknowledge J. P. Gauyacq for communicating his theoretical results in numerical form, A. Chutjian for discussions of his TPSA work, A. Chutjian, F. B. Dunning and D. Field for providing preprints, and S. Schohl for fruitful experimental cooperation. One of us (H. H.) thanks the Deutsche Forschungsgemeinschaft for travel support, enabling him to attend the Joint Symposium at Bond University, and is grateful to S. J. Buckman, R. W. Crompton and M. T. Elford for their hospitality.

References

Ajello, J. M., and Chutjian, A. (1979). *J. Chem. Phys.* **71**, 1079.

Alajajian, S. H., Bernius, M. T., and Chutjian, A. (1988). *J. Phys.* B **21**, 4021.

Astruc, J. P., Barbé, R., Lagrèze, A., and Schermann, J. P. (1983). *Chem. Phys.* **75**, 405.

Beterov, I. M., Vasilenko, G. L., Riabtsev, I. I., Smirnov, B. M., and Fateyev N. V. (1987). *Z. Phys.* D **6**, 55.

Bethe, H. A. (1935). *Phys. Rev.* **47**, 747.

Brincourt, G., Rajab Pacha, S., Catella, R., Zerega, Y., and André, J. (1989). *Chem. Phys. Lett.* **156**, 573.

Chang, T. N., and Kim, Y. S. (1982). *Phys. Rev.* A **26**, 2728.

Christophorou, L. G. (1978). *Adv. Electr. Electron Phys.* **46**, 71.

Christophorou, L. G. (Ed.) (1984). 'Electron Molecule Interactions and Their Applications', Vols 1 and 2 (Academic: New York).

Christophorou, L. G., James, D. R., and Pai, R. Y. (1982). *In* 'Applied Atomic Collision Physics', Vol. 5, pp. 87ff. (Academic: New York).

Chutjian, A. (1992). Invited Lecture at 17th ICPEAC, Brisbane (July 1991); to be published in 'Electronic and Atomic Collisions' (Proc. 17th ICPEAC).
Chutjian, A., and Alajajian, S. H. (1985). *Phys. Rev.* A **31**, 2885.
Chutjian, A., and Alajajian, S. H. (1987). *Phys. Rev.* A **35**, 4512.
Chutjian, A., Alajajian, S. H., Ajello, J. M., and Orient, O. J. (1984). *J. Phys.* B **17**, L745; *corrigendum* **18**, 3025.
Desfrançois, C., Khelifa, N., Lisfi, A., and Schermann, J. P. (1989). *J. Chem. Phys.* **91**, 5853.
Dunning, F. B. (1987). *J. Phys. Chem.* **91**, 2244.
Dunning, F. B., and Stebbings, R. F. (1974). *Phys. Rev.* A **9**, 2378.
Duzy, C., and Hyman, H. A. (1980). *Phys. Rev.* A **22**, 1878.
Fenzlaff, G., Gerhard, R., and Illenberger, E. (1988). *J. Chem. Phys.* **88**, 149.
Field, D., Knight, D. W., Mrotzek, G., Randell, J., Lunt, S. L., Ozenne, J. B., and Ziesel, J. P. (1991). *Meas. Sci. Technol.* **2**, 757.
Field, D., Mrotzek, G., Knight, D. W., Lunt, S. L., and Ziesel, J. P. (1988). *J. Phys.* B **21**, 171.
Gallagher, A. C., and York, G. (1974). *Rev. Sci. Instrum.* **45**, 662.
Ganz, J., Lewandowski, B., Siegel, A., Bussert, W., Waibel, H., Ruf, M.-W., and Hotop, H. (1982). *J. Phys.* B **15**, L485.
Gauyacq, J. P., and Herzenberg, A. (1984). *J. Phys.* B **17**, 1155.
Harmin, D. A. (1984). *Phys. Rev.* A **30**, 2413.
Harth, K., Raab, M., and Hotop, H. (1987). *Z. Phys.* D **7**, 213.
Harth, K., Ruf, M.-W., and Hotop, H. (1989). *Z. Phys.* D **14**, 149.
Hotop, H., and Lineberger, W. C. (1973). *J. Chem. Phys.* **58**, 2379.
Hotop, H., Patterson, T. A., and Lineberger, W. C. (1973). *Phys. Rev.* A **8**, 762.
Hunter, S. R., Carter, J. G., and Christophorou, L. G. (1989). *J. Chem. Phys.* **90**, 4879.
Kennerly, R. E., van Brunt, R. J., and Gallagher, A. C. (1981). *Phys. Rev.* A **23**, 2430.
Klar, D., Harth, K., Ganz, J., Kraft, T., Ruf, M.-W., and Hotop, H. (1991). Proc. Seminar on Today and Tomorrow of Photoionisation, Leningrad, April 1990, DL/SCI/R29, SERC Daresbury (Eds M. Ya. Amusia and J. B. West), p. 78.
Klar, D., Ruf, M.-W., and Hotop, H. (1992). *Chem. Phys. Lett.* **189**, 448.
Kline, L. E., Davies, D. K., Chen, C. L., and Chantry, P. J. (1979). *J. Appl. Phys.* **50**, 6789.
Klots, C. E. (1976). *Chem. Phys. Lett.* **38**, 61.
Kraft, T. (1991). Dissertation, Universität Kaiserslautern (unpublished).
Kraft, T., Ruf, M.-W., and Hotop, H. (1989). *Z. Phys.* D **14**, 179.
Kraft, T., Ruf, M.-W., and Hotop, H. (1990). *Z. Phys.* D **17**, 37.
Langevin, P. (1905) *Ann. Chim. Phys.* **5**, 245.
Ling, X., Lindsay, B. G., Smith, K. A., and Dunning, F. B. (1992). *Phys. Rev.* A **45**, 242.
Märk, T. D. (1991). *Int. J. Mass Spectrom. Ion Proc.* **107**, 143.
Matsuzawa, M. (1983). *In* 'Rydberg States of Atoms and Molecules' (Eds R. F. Stebbings and F. B. Dunning), pp. 267 ff. (Cambridge Univ. Press).
Nelson, Jr, R. D., and Cole, R. H. (1971). *J. Chem. Phys.* **54**, 4033.
Neukammer, J., Rinneberg, H., Vietzke, K., König, A., Hieronymus, H., Kohl, M., Grabka, H.-J., and Wunner, G. (1987). *Phys. Rev. Lett.* **59**, 2947.
O'Malley, T. F. (1965). *Phys. Rev.* **137**, A1668.
Oster, T., Kühn, A., and Illenberger, E. (1989). *Int. J. Mass. Spectrom. Ion Proc.* **89**, 1.
Petrović, Z. Lj., and Crompton, R. W. (1985). *J. Phys.* B **17**, 2777.
Randell, J., Field, D., Lunt, S. L., Mrotzek, G., and Ziesel, J. P. (1992). Submitted for publication.
Rohr, K. (1977). *J. Phys.* B **10**, 1175.
Schohl, S., Klar, D., Kraft, T., Meijer, H. A. J., Ruf, M.-W., Schmitz, U., Smith, S. J., and Hotop, H. (1991). *Z. Phys.* D **21**, 25.
Schohl, S., Klar, D., Kraft, T., Ruf, M.-W., and Hotop, H. (1992). *Verhandl. DPG (VI)* **27**, 1257.
Schulz, G. J. (1973). *Rev. Mod. Phys.* **45**, 423.
Vogt, E., and Wannier, G. H. (1954). *Phys. Rev.* **95**, 1190.
Weissmann, G., Ganz, J., Siegel, A., Waibel, H., and Hotop, H. (1984). *Opt. Commun.* **49**, 335.

Wigner, E. P. (1948). *Phys. Rev.* **73**, 1002.
Yoshihara, A., Anderson, A., Aziz, R. A., and Lin, C. C. (1980). *Chem. Phys.* **51**, 141.
Zollars, B. G., Higgs, C., Lu, F., Walter, C. W., Gray, L. G., Smith, K. A., Dunning, F. B., and Stebbings, R. F. (1985). *Phys. Rev.* A **32**, 3330.
Zollars, B. G., Walter, C. W., Lu, F., Johnson, C. B., Smith, K. A., and Dunning, F. B. (1986). *J. Chem. Phys.* **84**, 5589.

Manuscript received 5 March, accepted 11 May 1992